Length Scale Heterogeneity in Lateral Gradients of Poly(N -isopropylacrylamide) Polymer Brushes Prepared by Surface-Initiated Atom Transfer Radical Polymerization Coupled with In-...

ARTICLE *in* LANGMUIR · FEBRUARY 2006

Impact Factor: 4.46 · DOI: 10.1021/la052741p · Source: PubMed

Length Scale Heterogeneity in Lateral Gradients of Poly(*N*-isopropylacrylamide) Polymer Brushes Prepared by Surface-Initiated Atom Transfer Radical Polymerization Coupled with In-Plane Electrochemical Potential Gradients

Xuejun Wang, Huilin Tu, Paul V. Braun, and Paul W. Bohn*

Department of Chemistry, Department of Materials Science and Engineering, Beckman Institute for Advanced Science and Technology and Frederick Seitz Materials Research Laboratory, University of Illinois at Urbana-Champaign, 600 South Mathews Avenue, Urbana, Illinois 61801

Received October 10, 2005

We report the preparation and characterization of poly(*N*-isopropylacrylamide) (PNIPAAm) polymer brushes exhibiting controlled lateral variations in the patchiness of polymer chains. These gradients were achieved through an atom transfer radical polymerization (ATRP) grafting-from approach utilizing surfaces on which the spatial profile of the initiator density was carefully controlled. Initiator density gradients were formed on Au by first preparing a hexadecanethiol (HDT) density gradient, by reductive desorption using a laterally anisotropic electrochemical gradient. The bare areas in the original HDT gradient were then back-filled with a disulfide initiator, $(BrC(CH_3)_2COO(CH_2)_{11}S)_2$. The initiator coverage was characterized by X-ray photoelectron spectroscopy (XPS). Then, surface-initiated ATRP was utilized to transfer the initiator density gradient into gradients of PNIPAAm chain density. Ellipsometry, surface plasmon resonance (SPR), and atomic force microscopy (AFM) were used to characterize these PNIPAAm density gradients. The defining characteristic of the PNIPAAm gradients is the evolution of the morphology from discontinuous mushroom structures at extremely low grafting densities to heterogeneous patchy structures at intermediate grafting densities. The size of the patchy domains gradually increases, until at a high grafting density region, the morphology evolves to a smoother, presumably more extended, structure.

Introduction

This work explores the properties of lateral in-plane gradients of the thermally responsive hydrogel, poly(*N*-isopropylacrylamide), PNIPAAm, prepared by mapping a thiolated initiator onto the surface of a Au working electrode via a spatial gradient in the reductive desorption potential. The resulting PNIPAAm gradient structures exhibit lateral variations in grafting density, dry film thickness, and, most importantly, molecular organization, making them unique platforms with which to study the dependence of materials properties on structural organization.

Recently, there has been a great deal of interest in generating and utilizing gradient surfaces due to their myriad possible applications, such as forming substrates for selective adsorption, templates for cell migration, and tools for combinatorial chemistry studies. A number of techniques to generate gradients on various substrates have been reported, including diffusion controlled vapor deposition,[1] cross diffusion,[2,3] corona discharge,[4,5] photoimmobilization,[6,7] the use of microfluidic devices,[8,9] and, more recently, surface-initiated polymerization through atom transfer radical polymerization (ATRP).[10−17] ATRP is of special interest due to its versatility, robustness, controllability, and the living nature of the polymerization.[18−21] The use of surface-grafted polymers to control surface properties is attractive, so extensive research has been dedicated to understanding the behavior of tethered polymer chains at interfaces. For instance, combinatorial approaches to surface-initiated polymerization through ATRP have been used to probe the effects of graft density[10,13] and molecular weight[14,15] on polymer brush surfaces.

In our laboratory, an electrochemical−potential−gradient-based method has been developed to generate chemical composition gradients on thin Au electrodes.[22−29] In this method, the

* Corresponding author. E-mail: bohn@scs.uiuc.edu.

(1) Chaudhury, M. K.; Whitesides, G. M. *Science* **1992**, *256*, 1539−1541.
(2) Liedberg, B.; Tengvall, P. *Langmuir* **1995**, *11*, 3821−387.
(3) Liedberg, B.; Wirde, M.; Tao, Y.-T.; Tengvall, P.; Gelius, U. *Langmuir* **1997**, *13*, 5329−5334.
(4) Jeong, B. J.; Lee, J. H.; Lee, H. B. *J. Colloid Interface Sci.* **1996**, *178*, 757−763.
(5) Lee, J. H.; Kim, H. G.; Khang, G. S.; Lee, H. B.; Jhon, M. S. *J. Colloid Interface Sci.* **1992**, *151*, 563−570.
(6) Hypolite, C. L.; McLernon, T. L.; Adams, D. N.; Chapman, K. E.; Herbert, C. B.; Huang, C. C.; Distefano, M. D.; Hu, W.-S. *Bioconjugate Chem.* **1997**, *8*, 658−663.
(7) Herbert, C. B.; McLernon, T. L.; Hypolite, C. L.; Adams, D. N.; Pikus, L.; Huang, C. C.; Fields, G. B.; Letourneau, P. C.; Distefano, M. D.; Hu, W.-S. *Chem. Biol.* **1997**, *4*, 731−737.
(8) Jeon, N. L.; Dertinger, S. K. W.; Chiu, D. T.; Choi, I. S.; Stroock, A. D.; Whitesides, G. M. *Langmuir* **2000**, *16*, 8311−8316.
(9) Dertinger, S. K. W.; Jiang, X.; Li, Z.; Murthy, V. N.; Whitesides, G. M. *Proc. Natl. Acad. Sci. U.S.A.* **2002**, *99*, 12542−12547.
(10) Wu, T.; Efimenko, K.; Vlcek, P.; Subr, V.; Genzer, J. *Macromolecules* **2003**, *36*, 2448−2453.
(11) Bhat, R. R.; Tomlinson, M. R.; Genzer, J. *Macromol. Rapid Commun.* **2004**, *25*, 270−274.
(12) Bhat, R. R.; Genzer, J.; Chaney, B. N.; Sugg, H. W.; Liebmann-Vinson, A. *Nanotechnology* **2003**, *14*, 1145−1152.
(13) Wu, T.; Efimenko, K.; Genzer, J. *J. Am. Chem. Soc.* **2002**, *124*, 9394−9395.
(14) Tomlinson, M. R.; Genzer, J. *Chem. Commun.* **2003**, 1350−1351.
(15) Tomlinson, M. R.; Genzer, J. *Macromolecules* **2003**, *36*, 3449−3451.
(16) Zhao, B. *Langmuir* **2004**, *20*, 11748−11755.
(17) Xu, C.; Wu, T.; Drain, C. M.; Batteas, J. D.; Beers, K. L. *Macromolecules* **2005**, *38*, 6−8.
(18) Patten, T. E.; Matyjaszewski, K. *Adv. Mater.* **1998**, *10*, 901−915.
(19) Patten, T. E.; Xia, J.; Abernathy, T.; Matyjaszewski, K. *Science* **1996**, *272*, 866−868.
(20) Matyjaszewski, K.; Patten, T. E.; Xia, J. *J. Am. Chem. Soc.* **1997**, *119*, 674−680.
(21) Matyjaszewski, K.; Miller, P. J.; Shukla, N.; Immaraporn, B.; Gelman, A.; Luokala, B. B.; Siclovan, T. M.; Kickelbick, G.; Vallant, T.; Hoffmann, H.; Pakula, T. *Macromolecules* **1999**, *32*, 8716−8724.
(22) Terrill, R. H.; Balss, K. M.; Zhang, Y.; Bohn, P. W. *J. Am. Chem. Soc.* **2000**, *122*, 988−989.
(23) Balss, K. M.; Coleman, B. D.; Lansford, C. H.; Haasch, R. T.; Bohn, P. W. *J. Phys. Chem. B* **2001**, *105*, 8970−8978.

10.1021/la052741p CCC: $33.50
Published on Web 12/03/2005

in-plane current is injected at one end of an ultrathin (5 nm ≤ d ≤ 80 nm) Au film and collected at the other end, while the Au film is used simultaneously as the working electrode of an electrochemical cell. Injection of currents yields significant in-plane potential drops so that, rather than assuming a single value of potential, an in-plane potential gradient, $V(x)$, is imposed on the working electrode surface according to

$$V(x) = V_0 + \int \frac{i\rho(l)}{A} dl \quad (1)$$

where V_0 is the potentiostat voltage offset, i is the magnitude of the injected current, $\rho(l)$ is the film resistivity, and A is the cross-sectional area of the Au working electrode. The in-plane potential gradient can be exploited to map organothiols onto the Au electrode surface by using the characteristic reductive desorption/oxidative adsorption reactions of alkanethiols. In contrast to other preparation methods, this approach can be applied to samples with a broad range of physical sizes; it is easy to tune gradient properties such as transition position and slope; and the gradients may be altered after initial formation, thereby yielding spatial and temporal control over the surface composition, $\Gamma(x,y,t)$. By first forming a one-component organothiol gradient and then refilling the initial gradient with a second thiol or disulfide, two-component gradients can also be generated. These one- or two-component gradients can then be further derivatized at the solvent-accessible outer surface, for example, with various biomacromolecules, such as fibronectin, through covalent linkage.[26]

Understanding the effect of polymer brush domain size on materials properties is of fundamental interest. Surface-initiated polymerization through ATRP can be used to produce grafting density and molecular weight gradients of polymer brushes on flat SiO_2. Combining ATRP with electrochemically derived composition gradients offers the possibility of controlling the nanometer lengthscale segregation, so as to produce polymer brush gradients with gradually changing domain sizes on Au. Thus, in the present work, a spatial gradient of the disulfide initiator, $(BrC(CH_3)_2COO(CH_2)_{11}S)_2$, **I**, is generated on the Au substrate by first generating a gradient in the coverage of a hexadecanethiol, HDT, monolayer, then filling in the bare areas with initiator. The surface initiator density gradient is then utilized, through ATRP, to form PNIPAAm brushes, displaying a laterally varying domain size, with the spatially inhomogeneous PNIPAAm domains being attributed to inhomogeneous distribution of the initiator, generated during the gradient formation process.

PNIPAAm is one of the most studied environmentally responsive materials due to its well-known lower critical solution temperature (LCST) transition of ∼30 °C in aqueous solutions.[30,31] Free PNIPAAm chains in pure water undergo a sharp LCST phase transition at 32 ± 1−2 °C. In contrast, when PNIPAAm is grafted to a solid surface, a broadened LCST transition is observed.[32,33] The general LCST behavior of end-graftedPNIPAAm is thought to be dependent on two critical brush parameters, grafting density, and molecular weight of the polymers.[34,35] This work is focused on the PNIPAAm polymer brush system; however, the polymer brush gradient formation strategy reported here is quite general, meaning that any material amenable to ATRP growth can be templated using electrochemically formed initiator gradients. This strategy is not limited by the physical size of the substrate down to the micrometer scale, depending only on the length over which the electrochemical potential gradient is applied. It may also be extended to form two-component gradients since the HDT remaining after polymerization can be selectively removed by applying a uniform reductive desorption potential. Then, the bare areas can be refilled with initiator for another round of ATRP with a different monomer, making it possible to form block copolymer brush gradients. By taking advantage of the nature of gradual variations in polymer brush domain size, various types of polymer brushes with different domain sizes can be studied in a single sample.

Results and Discussion

Formation and Characterization of PNIPAAm Brush Density Gradients. The strategy for the formation of PNIPAAm density gradients builds on the grafting-from ATRP approach for preparing spatially uniform PNIPAAm films on Au, described in the Supporting Information, and is presented in Figure 1. It consists of three steps: (1) preparation of HDT areal density gradients using the electrochemical potential gradient method, (2) formation of initiator density gradients by refilling the areas denuded of HDT with a disulfide initiator, and (3) generation of PNIPAAm density gradients through surface-initiated ATRP. An alternative strategy for generating initiator density gradients would be to map electrochemical potential gradients into SAMs of initiator $(BrC(CH_3)_2COO(CH_2)_{11}S)_2$ (**I**) on Au directly. However, here the disulfide initiator **I** was used to backfill an originally formed gradient in HDT to minimize the exchange of initiator molecules with HDT molecules on the Au surface[36] and because **I** hydrolyzes in 0.5 M KOH.

Figure 2 shows a series of spatially resolved XPS spectra in the C 1s and O 1s regions acquired from nine equally separated positions along the 30 mm long active transition region of an initiator gradient. Figure 2a shows that the shape of the C 1s peak gradually evolves from being symmetrical at the high HDT coverage end to asymmetry at the low HDT coverage end. The asymmetric C 1s peak at the low HDT density end of the gradient can be fit with three components: (1) a peak around 288.5 eV corresponding to unsaturated carbon in the carbonyl group, (2) a band near 285.6 eV due to a carbon adjacent to the carbonyl group and carbon in the $-OCH_2$ unit, and (3) a band at ∼284.7 eV attributed to saturated carbon in the alkyl chain. The evolution of the O 1s band is shown in Figure 2b. The O 1s peaks can be fit with two bands: one at 531.6 eV that is attributed to the carbonyl oxygen and the peak at 533.0 eV that is due to a single bonded $-OCH_2$ oxygen. The normalized integrated areas of the O 1s and C 1s XPS bands are shown as a function of position in Figure 3. The O 1s intensity gradually increases from the

(24) Balss, K. M.; Fried, G. A.; Bohn, P. W. *J. Electrochem. Soc.* **2002**, *149*, C450−C455.
(25) Balss, K. M.; Kuo, T.-C.; Bohn, P. W. *J. Phys. Chem. B* **2003**, *107*, 994−1000.
(26) Plummer, S. T.; Wang, Q.; Bohn, P. W.; Stockton, R.; Schwartz, M. A. *Langmuir* **2003**, *19*, 7528−7536.
(27) Plummer, S. T.; Bohn, P. W. *Langmuir* **2002**, *18*, 4142−4149.
(28) Wang, Q.; Bohn, P. W. *J. Phys. Chem. B* **2003**, *107*, 12578−12584.
(29) Wang, Q.; Jakubowski, J. A.; Sweedler, J. V.; Bohn, P. W. *Anal. Chem.* **2004**, *76*, 1−8.
(30) Schild, H. G. *Prog. Polym. Sci.* **1992**, *17*, 163−249.
(31) Katsumoto, Y.; Tanaka, T.; Sato, H.; Ozaki, Y. *J. Phys. Chem. A* **2002**, *106*, 3429−3435.
(32) Zhu, P. W.; Napper, D. H. *J. Colloid Interface Sci.* **1994**, *164*, 489−494.
(33) Balamurugan, S.; Mendez, S.; Balamurugan, S. S.; O'Brien, M. J.; Lopez, G. P. *Langmuir* **2003**, *19*, 2545−2549.
(34) Yim, H.; Kent, M. S.; Mendez, S.; Balamurugan, S. S.; Balamurugan, S.; Lopez, G. P.; Satija, S. *Macromolecules* **2004**, *37*, 1994−1997.
(35) Mendez, S.; Curro, J. G.; McCoy, J. D.; Lopez, G. P. *Macromolecules* **2005**, *38*, 174−181.
(36) The exchange rate of disulfide to thiol is two magnitudes slower than the thiol to thiol exchange, as shown in Abbott, N. L.; Folkers, J. P.; Whitesides, G. M. *Science* **1992**, *257*, 1380−1382.

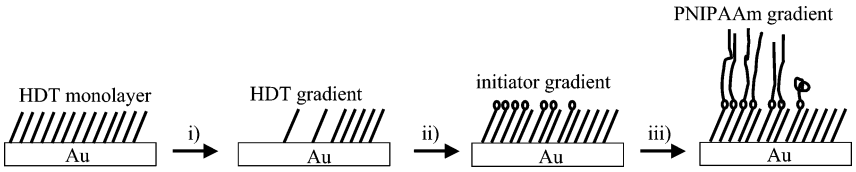

Figure 1. Strategy for mapping a laterally varying density gradient of the initiator, **I**, into a PNIPAAm chain density gradient. (i) Spatially dependent desorption of the initially formed HDT SAM. (ii) Disulfide initiator **I** is backfilled into the bare areas in the HDT SAM. (iii) Surface-initiated ATRP production of PNIPAAm. In the last stage, the chain morphology is dependent on the number of neighboring chains.

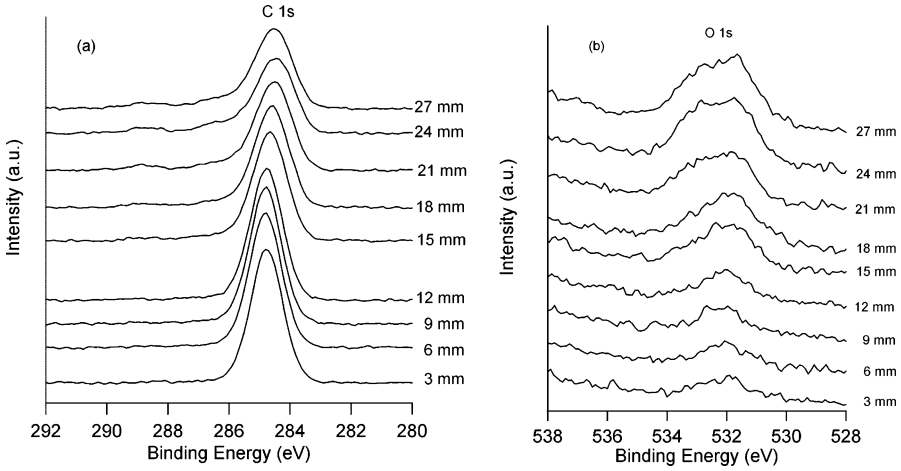

Figure 2. Series of spatially resolved XPS spectra in the C 1s (a) and O 1s (b) spectral regions acquired from nine equally separated positions along the 30 mm long active transition region of an initiator gradient. The position labeled 3 mm corresponds to the low initiator coverage end, and the position labeled 27 mm corresponds to the high initiator coverage end.

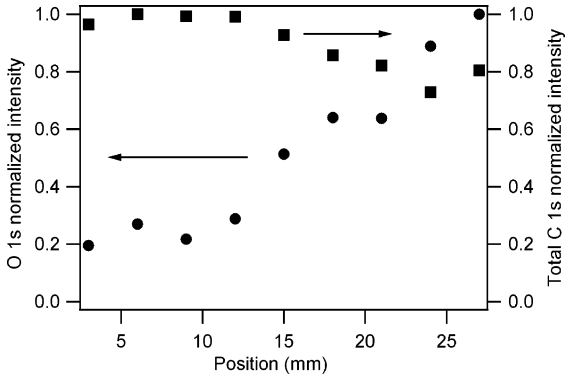

Figure 3. Normalized integrated areas of the o 1S (●) and C 1s (■) XPS bands as a function of spatial position obtained from the initiator gradient.

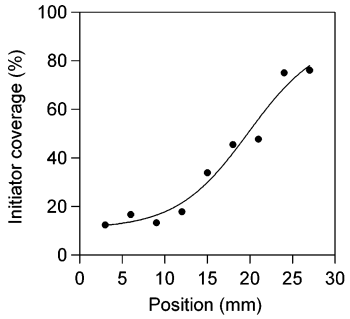

Figure 4. Initiator coverage determined from the O/C ratio as a function of position for the initiator gradient. The symbols give the measured coverage, and the error bars represent ±1 standard deviation. The solid line is a fit of the data to a sigmoidal function.

position of 12 mm to 30 mm, as a result of the formation of the initiator gradient. The C 1s intensity change is less dramatic; it slightly decreases going toward the high initiator end of the gradient, consistent with the less packing property of the initiator SAM relative to HDT SAM.

The fractional coverage, α, of the initiator, **I**, in the gradient can be estimated from the XPS data by comparing the O/C ratio from the initiator gradient to that from a full SAM of **I**, which is measured to be 0.18. Given that the Au surface is covered with (1-α) of HDT and α of the initiator, the ratio of the stoichiometric O/C ratio in the gradient sample to the stoichiometric O/C ratio in a fully covered initiator is theoretically $15\alpha/(16-\alpha) \approx \alpha$. Taking photoelectron attenuation effects into account, a semiempirical calculation by Liedberg et al.[3] yields the corresponding fraction value to be $12.8\alpha/(13.4-0.6\alpha) \approx \alpha$. Thus, the relative initiator coverage is approximately the ratio of the O/C ratio in the gradient sample to the O/C ratio in a fully covered initiator SAM. Figure 4 shows the calculated relative initiator coverage at different positions. The solid line is a fit of the experimental data to a sigmoidal function

$$\alpha(x) = \alpha_b + \frac{\alpha_{max}}{1 + e^{(x_0 - x)/r}} \qquad (2)$$

where α_b is a coverage offset, α_{max} is the normalized maximum coverage, x_0 is the inflection point of the slope region, and r is a spatial rate constant related to the slope.

The PNIPAAm chain density gradients were generated by exposing the initiator density gradient formed on Au/Silicon or Au/SF10 glass to CuBr/ligand/NIPAAm in 1:1 MeOH/H_2O. Ellipsometry was used to measure the thickness of the dry polymer film, h, as a function of position on the substrate. Since no deactivator ($CuBr_2$) was added, it is not surprising that the PNIPAAm polymer brush thickness varies from batch to batch.[37] However, in this work, the polymer brush thickness as a function of the lateral position is the relevant quantity, so precise thickness control was not needed. Figure 5, which displays h from eight

(37) Matyjaszewski, K.; Shipp, D. A.; Wang, J. L.; Grimaud, T.; Patten, T. E. *Macromolecules* **1998**, *31*, 6836−6840.

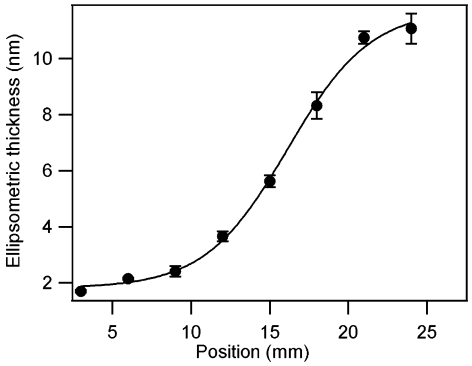

Figure 5. Ellipsometric thickness in air from eight equally separated positions along the 30 mm long active transition region of a PNIPAAm density gradient formed by surface-initiated ATRP of NIPAAm on an initiator density gradient sample for 90 min. The solid line is a fit to a sigmoidal function.[43]

equally spaced positions along the 30 mm long active transition region of a PNIPAAm density gradient formed by surface-initiated ATRP of NIPAAm on an initiator density gradient shows that the ellipsometric thickness, *h*, increases gradually from the low initiator density end of the gradient (position 0 mm) to the high initiator density end (position 30 mm). The spatial variation in *h* clearly matches the spatial variation in initiator coverage shown in Figure 4. The grafting density of polymer brush phases can be calculated from

$$\sigma = \frac{h\rho N_A}{M_n} \tag{3}$$

where ρ is the density of PNIPAAm, N_A is Avogadro's number, and M_n is the polymer molecular weight. Considering the highly controlled nature of ATRP, it is reasonable to assume that the polymers grafted to the initiator density gradient sample have the same degree of polymerization.[10,38] Consistent with Huck and co-workers' study of the effect of initiator density on the polymerization of poly(methyl methacrylate) using ATRP,[38] the dry polymer film thickness is proportional to the grafting density of the PNIPAAm polymer brush. Thus, the concordance of the initiator coverage gradient (Figure 4) with the PNIPAAm thickness gradient (Figure 5) indicates that the grafting density of the polymer scales monotonically with the original areal density of the initiator.

SPR imaging, because it reports on the spatial distribution of the optical response function, can provide information about PNIPAAm density gradients complementary to that obtained from ellipsometry. To measure the angle shift of the PNIPAAm films with a different polymer grafting density at the same time, the sample was mounted to a 60° prism in the Kretschmann configuraton in such a way that the grafting density increases from top to bottom, as shown schematically in Figure 6 a. SPR imaging of the PNIPAAm chain density gradient with an incoherent white light source/narrow band interference filter combination[39] produced images typified by that shown in Figure 6b. Figure 6c shows both the SPR angle shift and the ellipsometrically determined dry film thickness as a function of spatial position along the gradient sample. From Figure 6b,c, it is clear that the surface areal density of the initiator is mapped directly into the grafting density of the PNIPAAm chains. The SPR angle shift reports on the total dielectric response function,

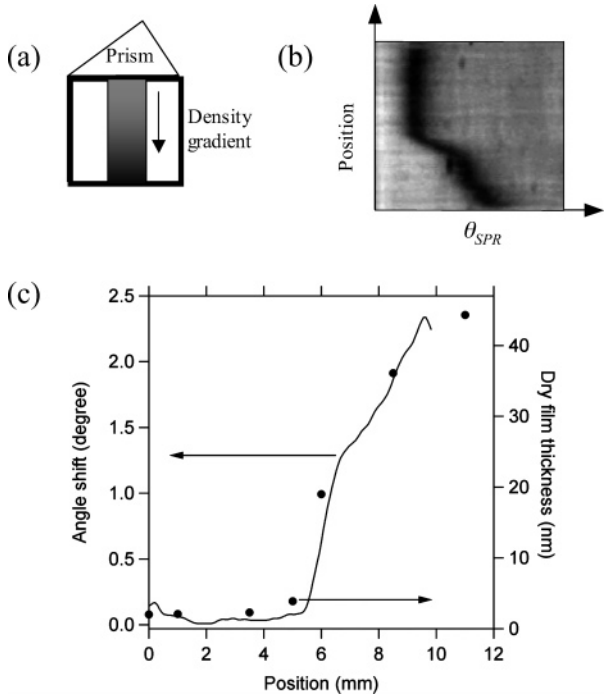

Figure 6. (a) Schematic diagram of the SPR imaging arrangement to visualize the PNIPAAm gradient sample by mounting it on a 60° prism in the Kretschmann configuration. The chain grafting density increases from top to bottom. (b) Typical SPR angle shift image of a PNIPAAm density gradient. (c) SPR angle shift (—) and ellipsometric thickness (●) as a function of spatial position along the gradient sample.

which in turn is attributed to a combination of the change in wet film thickness and the index of the polymer. For comparison, the dry polymer thickness of the same sample measured from ellipsometry in air, shown in Figure 6c, matches the spatial variation in the SPR angle shift very well. The excellent agreement of the wet (SPR) and dry (ellipsometry) film profiles is further evidence for the integrity of the spatial mapping of the initiator gradient into a PNIPAAm chain density gradient.

Morphology of PNIPAAm Brush Gradients. AFM studies of PNIPAAm density gradients were performed to determine the morphology of polymer brushes at different grafting density regions. Ultra-flat template-stripped Au substrates (1 cm × 1 cm) were used to reduce background noise and allow the PNIPAAm morphology to be accurately measured. The initiator gradient was generated by applying an electrochemical potential gradient (−1400 mV at $x = 0$ mm to −400 mV at $x = 10$ mm) to an HDT SAM, after which the bare areas were refilled with **I**. Figure 7 shows the fit of the initiator coverage as a function of position to the sigmoidal function determined from Figure 4. The initiator density decreases from $x = 0$ mm to $x = 10$ mm, signaling that the grafting density of polymer brushes after ATRP reaction decreases correspondingly. AFM images and corresponding line scans at $x = 1$, 3, 5, 7, and 9 mm of a typical PNIPAAm density gradient are shown as insets in Figure 7. The RMS roughness at $x = 9$ mm is 1.45 nm, indicating that the underlying template-stripped Au surface is exceptionally smooth. The sparse population of small clusters with ~10 nm height and 130 nm diameter in the $x = 9$ mm image are likely well-separated polymer mushrooms formed on the extremely low initiator coverage region (initiator coverage ~12%). Progressing across the sample to higher initiator density regions, the RMS roughness of the images at $x = 7$ and 5 mm are 7.80 and 3.06 nm, respectively. These roughness measurements and the ca. 300−500 nm domain size determined from the tapping mode images suggest that patchy

(38) Jones, D. M.; Brown, A. A.; Huck, W. T. S. *Langmuir* **2002**, *18*, 1265−1269.

(39) Brockman, J. M.; Nelson, B. P.; Corn, R. M. *Annu. Rev. Phys. Chem.* **2000**, *51*, 41−63.

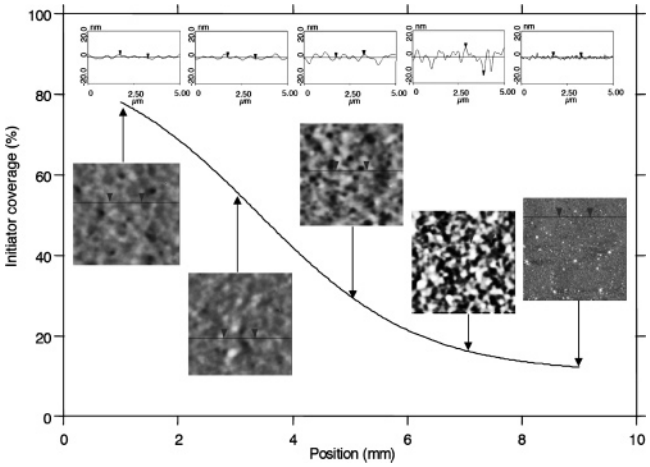

Figure 7. Relationship of PNIPAAm film morphology to local grafting density as tracked through the initiator density. The solid line gives the initiator coverage as a function of position. Individual insets show 5 μm × 5 μm tapping mode AFM topography images and section analysis line scans (above the respective images) at x = 1, 3, 5, 7, and 9 mm of a 10 mm long PNIPAAm density gradient.

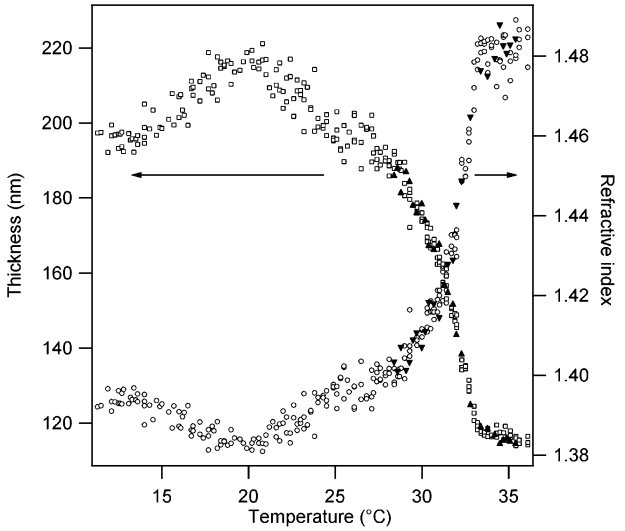

Figure 8. Thickness and refractive index of PNIPAAm brushes as a function of temperature as determined by environmental ellipsometry. (□) Thickness during heating, (▲) thickness during cooling, (○) refractive index during heating, and (▼) refractive index during cooling.

structures are exhibited at intermediate grafting densities. The size of the patches increases from ∼300 nm at 16% initiator coverage to more than 500 nm at 30% initiator coverage. Images x = 3 and 1 mm show RMS roughness values of 1.51 and 1.59 nm, respectively, indicating that at high grafting density, the PNIPAAm film morphology is very smooth. Thus, the picture that emerges from the AFM studies is one in which the lateral variation in chain density is accompanied by a concomitant change in morphology, gradually evolving from discontinuous mushroom structures at extremely low grafting densities to heterogeneous patchy structures at intermediate grafting densities. The size of the patch structures gradually increases with increasing initiator coverage, until at high grafting density region the morphology evolves to a smoother, presumably more extended, structure.

Huck and co-workers' study of the effect of initiator density on polymerization of poly(methyl methacrylate) using ATRP showed a homogeneous polymer brush morphology with a larger grain size at a lower initiator coverage region for molecularly mixed initiator SAMs.[38] This observation contrasts with the heterogeneous nature of the PNIPAAm brush morphology reported here, suggesting that the distribution of initiator molecules in this work is different from that in the PMMA system. Thus, the AFM results here suggest that the initiator gradient consists of heterogeneously distributed patches of initiator molecules surrounded by HDT, with the smallest patches in the regions of lowest initiator coverage. This structure is likely templated at the HDT gradient formation stage because the reductive stripping of HDT, being a nucleated process, is expected to produce a patchy structure due to the energetic difference between removing HDT molecules from the center of a homogeneously populated region and removing an HDT molecule near the edge of a growing island.

Temperature Response of Uniform and Gradient PNIPAAm Brush Structures. The thermal response of uniform PNIPAAm brushes was tested by environmental ellipsometry. The PNIPAAm brush structures were prepared through ATRP in an overnight reaction. Figure 8 shows the thickness and refractive index of PNIPAAm brushes as a function of temperature. The crossover of the two curves occurs near their inflection points at 31.4 °C, which corresponds to the lower critical solution temperature (LCST), where the film exhibits a thickness of 157 nm and a refractive index of 1.42. Below the LCST, the thickness is larger and the refractive index smaller corresponding to a phase in which the PNIPAAm brushes are swollen in water. When the temperature is increased through the LCST, the PNIPAAm brushes contract, producing a dense phase that expels water, resulting in decreased thickness and increased refractive index. The LCST transition occurs over a broad temperature range of 20−35 °C, with the majority of the transition between 28 and 34 °C, consistent with the thermal response of ∼21 nm dry PNIPAAm brushes on silicon wafers observed by Tu et al.[40] Figure 8 shows that the behavior during heating and cooling cycles exhibits very little hysteresis in the LCST transition region, indicating the reversibility of this transition. Finally, there is a slight increase in thickness and a decrease in refractive index in the temperature range of 11−20 °C. Although small the effect is reproducible, we speculate that it might be due to a pre-LCST structural reorganization resulting in a solubility change of the PNIPAAm brushes.

For comparison, the temperature response of a ∼130 nm PNIPAAm film sample, prepared through ATRP overnight, was measured in water and in 0.5 M NaCl by SPR reflectometry. As shown in Figure 9, the LCST transition of PNIPAAm film in water occurs over a wide temperature range, 17−36 °C, with the majority of the transition between 28 and 34 °C and the center of the LCST transition at ∼32 °C. This result is consistent with ellipsometry measurements. In 0.5 M NaCl, the LCST transition of the PNIPAAm film shifts to a lower temperature range of 16−28 °C, with the major change between 19 and 27 °C and the center of the LCST transition at ∼25 °C. The decrease of LCST transition temperature in 0.5 M NaCl is due to the well-known salting-out effect.[41] It is worth noting the effect of the width of the LCST transition, as measured by SPR. Although broad, small shifts in the position of the LCST transition can still be determined by fitting the SPR data in the transition region and using the derivative of the fit function to differentiate between LCST transition temperatures. We conservatively estimate that even with the transitions observed here, we can differentiate between LCST values differing by as little as 0.5 °C.

(40) Tu, H.; Heitzman, C. E.; Braun, P. V. *Langmuir* **2004**, *20*, 8313−8320.
(41) Krasovitski, E.; Cohen, Y.; Bianco-Peled, H. *J. Polym. Sci., Part B:Polym. Phys.* **2004**, *42*, 3713−3720.

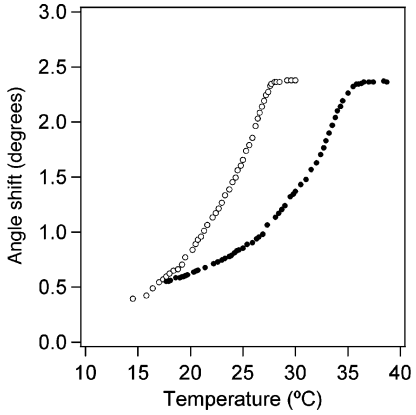

Figure 9. Temperature response of a ~130 nm uniform PNIPAAm film in water (●) and in 0.5 M NaCl (○) measured by SPR reflectometry.

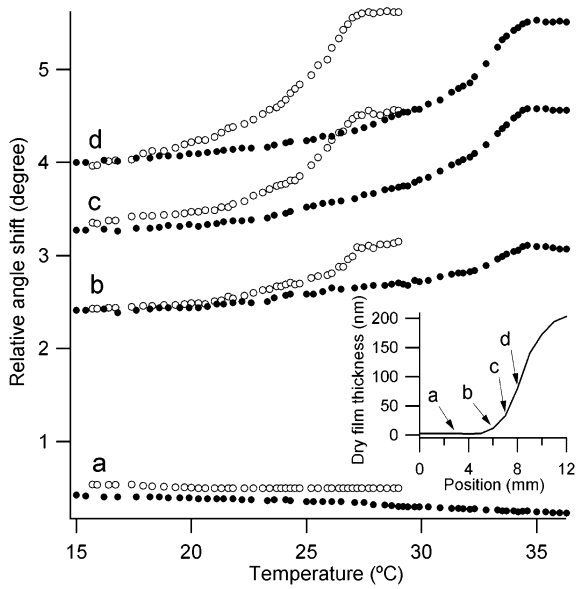

Figure 10. Temperature response of a PNIPAAm gradient sample in water (●) and 0.5 M NaCl (○) at positions with different PNIPAAm chain densities (positions a−d are taken from the ellipsometric film thickness gradient in the inset).

The temperature response of a PNIPAAm gradient sample in water and in 0.5 M aqueous NaCl was also measured with SPR to ascertain if the local density of polymer brush has any effect on the LCST transition for this specific PNIPAAm system. Using PNIPAAm gradients to study these phenomena has two advantages. First, because gradient surfaces are polymerized in the same reaction mixture, the resulting surface-bound PNIPAAm chains are members of the same molecular weight distribution. Thus, gradient samples can be prepared in which the coverage of polymer brushes gradually changes from one end to the other, while the polymer molecular weight remains constant. Second, by using one gradient sample, instead of several samples, the LCST transition temperature as a function of polymer brush coverage can be determined in a single measurement using imaging techniques, such as surface plasmon resonance (SPR) imaging.

Figure 10 shows the SPR temperature response of a PNIPAAm gradient sample at positions with different PNIPAAm chain densities (Figure 10a−d). The positions a−d are marked on the inset, which is the ellipsometric thickness of the gradient in air as a function of spatial position. Position a is located in the HDT region, and positions b−d are located in relatively low, medium, and high coverage PNIPAAm polymer brush regions, respectively. The grafting density of polymer brush at positions a−d can be calculated from eq 3. According to the literature, the average cross-sectional area of PNIPAAm chains, obtained from surface-initiated ATRP reactions using a fully covered ω-mercaptoundecylbromoisobutyrate as initiator, is ca. 200 Å^2 corresponding to a surface density of 5.0×10^{-3} chains/Å^2.[38,42] Assuming that M_n is the same for a gradient sample and that the thickest polymer end is fully covered with initiator, the surface chain density at positions a−d can be estimated to be 2.0×10^{-5}, 2.7×10^{-4}, 8.0×10^{-4}, and 2.0×10^{-3} chains/Å^2, respectively. At the nearly zero coverage characteristic of position a, the SPR resonance angle slightly decreases with increasing of temperature in water, which is ascribed to the decrease in the refractive index of water as a function of temperature.[33] The LCST transition of the PNIPAAm film at positions b−d in water happens over a wide temperature range of 20−35 °C, with the majority of the transition between 28 and 34 °C . The LCST transition does not shift from positions b−d, suggesting that the LCST transition is not affected by PNIPAAm polymer brush coverage in water. In 0.5 M NaCl, the LCST transition of the PNIPAAm film at positions b−d shifts to a lower temperature range of 16−28 °C, with the major change between 19 and 27 °C and the center of the LCST transition around 25 °C . Again, just as for DI water, no LCST transition shift is observed among positions b−d, indicating that the LCST transition is independent of the PNIPAAm polymer brush coverage in 0.5 M NaCl.

Recently Lopez et al. studied the effects of temperature, degree of polymerization, and surface coverage on the equilibrium structure of tethered PNIPAAm chains immersed in water with a self-consistent field approach based on density functional theory.[35] They predicted that surface coverage should have a dramatic effect on the LCST transition temperature, with higher surface coverages corresponding to lower transition temperatures. This is in contrast to the temperature response of the gradient sample reported here. One possible reason for the discrepancy is that the PNIPAAm brush gradients studied here, rather than being mixed homogeneously on the molecular length scale, consists of patchy structures of different sizes. Within each patch, the structure is homogeneous on a molecular scale, but the size and areal density of the patches is inhomogeneous on the 100 nm to 1 μm length scale, as revealed by AFM measurement, and of course, the number and density of patches varies laterally along the gradient.

Conclusions

We report a method for generating polymer brushes displaying spatially varying patches of PNIPAAm. The polymer brushes are prepared by ATRP starting from an initiator density gradient. The initiator density gradient is generated by spatially dependent reductive desorption of HDT, followed by refilling the denuded areas with a disulfide initiator, $(BrC(CH_3)_2COO(CH_2)_{11}S)_2$. Using this method to produce PNIPAAm grafting density gradients allows both the position and the slope of the PNIPAAm gradient to be readily controlled. Furthermore, the mapping of the chain density gradient onto the primary gradient of the initiator areal density is quite general, meaning that any material amenable to ATRP growth can be adapted to this gradient formation method. This gradient formation strategy is not limited by the physical size of the substrate, depending only on the length over which

(42) Kim, J. B.; Bruening, M. L.; Baker, G. L. *J. Am. Chem. Soc.* **2000**, *122*, 7616−7617.
(43) Wang, X. J.; Bohn, P. W. *J. Am. Chem. Soc.* **2004**, *126*, 6825−6832.

the electrochemical potential gradient is applied. Ellipsometry, SPR reflectometry and imaging, and AFM imaging were used to characterize these PNIPAAm density gradients. Thus, the picture that emerges from the spectroscopic and imaging studies is one in which the lateral variation in chain density is accompanied by a concomitant change in morphology, gradually evolving from discontinuous mushroom structures at extremely low grafting densities to patch structures at intermediate grafting densities. The size of the patch structures gradually increases with increasing initiator coverage, until at high grafting density, the morphology becomes a smoother, presumably extended structure. The temperature response of uniform and gradient PNIPAAm films in water shows similar LCST transition temperatures determined by ellipsometry and SPR reflectometry, indicating that the LCST transition is unaffected by the grafting density of the PNIPAAm chains, a result that reflects the importance of molecular-scale homogeneity within a film displaying overall heterogeneity on the nanometer to micrometer length scale.

Acknowledgment. This work was supported by the National Science Foundation through Grant CHE 0451661 and by the Department of Energy through Grant DE FG02 91ER45439. The Center for Microanalysis of Materials is partially supported by the Department of Energy through Grant DE FG02 91ER45439. Ellipsometry data were obtained in the Laser and Spectroscopy Facility at the Frederick Seitz Materials Research Laboratory.

Supporting Information Available: Experimental section, including materials, synthesis of $(BrC(CH_3)_2COO(CH_2)_{11}S)_2$ (I), experimental procedures, and characterization. Results for surface-initiated polymerization of spatially uniform PNIPAAm brush films. This material is available free of charge via the Internet at http://pubs.acs.org.

LA052741P